Analysis of an alternative semblance function applied to Finite-Offset Common-Reflection-Surface tomography

Marcelo Jorge Luz Mesquita (CPGF/UFPA) and João Carlos Ribeiro Cruz (IG/UFPA)

Abstract

Estimation of an accurate velocity model is a significant step in seismic processing. Finite-offset common-reflection-surface tomography is a layer-by-layer velocity inversion technique driven by the mean of global optimization. It is also part of a range of techniques known as coherence inversion methods. In this study, we are interested in analyzing this tomography technique considering an alternative semblance as the objective function. Our applications consist of both synthetic and field examples.

Introduction

Velocity model building is a relevant process to provide a reliable seismic image for interpreting geologic structures of interest. We have found in the geophysical literature many efforts to develop velocity inversion methods. Between them, we can cite the tomography methods in the time and depth domain (Goldin, 1979; Tarantola, 1984; Billete and Lambaré, 1998).

Finite-Offset Common-Reflection-Surface (FO CRS) tomography (Mesquita et al., 2019) is a layer-by-layer velocity inversion technique based on the FO CRS hyperbolic traveltime approximation and driven by mean of the global optimization algorithm Very Fast Simulated Annealing (VFSA) (Ingber, 1989). It is also part of a range of techniques known as coherence inversion methods, in which the objective function is given by a coherence measurement equation, in this case, the so-called semblance (Neidell and Taner, 1971).

Semblance is a relevant and reliable measure of coherence that has been used in seismic processing since the 1970s. Between many applications, we can cite the conventional velocity analysis and CRS stack technique. The well-known second-order semblance equation has proven to be quite robust and suitable for many situations. Besides, the literature has shown that higher-order coherence measures are quite successful in most different types of applications (Wiggins, 1978; Lu et al., 2005; Lima et al., 2011).

In this paper, we aim to analyze the behavior of the FO CRS tomography method, considering an alternative semblance as the objective function. For our objectives, we present two applications. The first one consists of a synthetic data set, where we show the possibility to reduce both the region of search and local minimum values. The second, a field data set, we study the convergence aspects of the method.

Theoretical aspects

FO CRS traveltime

Consider a central ray starting at a point *S* with initial velocity v_S and angle β_S. Consider now that it reflects at *R* in the subsurface and emerges, at the surface, in *G* with final velocity v_G and angle β_G. The traveltime of the finite-offset paraxial ray (Zhang et al., 2001), with $v_S = v_G = v_0$, is expressed by

$$T_{CRS}^2 = \left[t_0 + \left(\frac{1}{v_0}\right)(a_1\Delta x_m + a_2\Delta h)\right]^2 + \left(\frac{t_0}{v_0}\right)[a_3 - a_4]\Delta x_m^2 - \left(\frac{t_0}{v_0}\right)[a_4 - a_5]\Delta h^2 + 2\left(\frac{t_0}{v_0}\right)[a_4 + a_5]\Delta x_m \Delta h, \quad (1)$$

where $a_1 = \sin\beta_G + \sin\beta_S$, $a_2 = \sin\beta_G - \sin\beta_S$, $K = 4K_1 - 3K_3$, $a_3 = K\cos^2\beta_G$, $a_4 = K_2\cos^2\beta_S$ and $a_5 = K_3\cos^2\beta_G$. The traveltime along the central ray is given by t_0. The parameters β_S and β_G are the start and emergence angles of the central ray for the source *S* and the receiver *G* with coordinates x_S and x_G.

The quantities $\Delta x_m = x_m - x_0$ and $\Delta h = h - h_0$ correspond to the midpoint and half-offset displacements, where $x_0 = (x_G + x_S)/2$ is the midpoint and $h_0 = (x_G - x_S)/2$ is the half-offset of the central ray with finite-offset. The midpoint x_m and the half-offset h are the coordinates of an arbitrary paraxial ray with a finite-offset. The parameters K_1, K_2, and K_3, are the wavefront curvatures associated with the central ray, and they are calculated in the respective emergence points.

Considering that the common midpoint is common to the central and paraxial rays, the CMP condition implies $\Delta x_m = 0$, and the FO CRS traveltime approximation becomes (Callapino et al., 2011):

$$T_{CMP}^2 = \left[t_0 + \left(\frac{1}{v_0}\right)(a_2\Delta h)\right]^2 - \left(\frac{t_0}{v_0}\right)[a_4 - a_5]\Delta h^2. \quad (2)$$

Coherence measurement: Semblance

Frequently used in the seismic stack process, semblance (Neidell and Taner, 1971) is a coherence measurement that estimates the presence or absence of signals correlated along the traveltime curves calculated by FO CRS approximation in the CMP gathers.

For the FO CRS tomography applications, let us consider the following expression of the semblance function:

$$S(\mathbf{m}) = \frac{\sum_{k=-w}^{w}\left[\sum_{i=1}^{N} a_i(t_k)\right]^2}{N\sum_{k=-w}^{w}\left[\sum_{i=1}^{N} a_i(t_k)^2\right]}. \quad (3)$$

In this case, $\mathbf{m}$ represents the vector of parameters, given by $\mathbf{m} = \{\mathbf{V}, \mathbf{Z}(\mathbf{V}), \mathbf{W}(\mathbf{V}, \mathbf{Z})\}$, where $\mathbf{V}$ is the vector of velocities, $\mathbf{Z}$ is the vector of depths, and $\mathbf{W} = (t_o, K_2, K_3, \beta_s, \beta_g)$. Here, $a_i(t_k)$ is the seismic signal amplitude indexed by the trace order number i and in the function of the time t. This time is indexed by k, which falls in a given time window of width $2w + 1$. The value of the semblance function varies between 0 and 1. So, the closer to 1 its value, the better is the model obtained.

In the FO CRS tomography strategy, we adopt as the objective function, given by $E(\mathbf{m})$, the arithmetic mean of all semblances values calculated in a layer, that is

$$E(\mathbf{m}) = \frac{1}{L}\sum_{j=1}^{L}[S(\mathbf{m})]_j, \quad (4)$$

where L is the number of CMP gathers analyzed per layer.

Methodology

For our study, we apply the algorithm of velocity inversion, which involves the application of various techniques, as described below:

1. Time horizon picking at stacked or migrated section to obtain the reflection times of events that describe interfaces;
2. Time to depth conversion using normal- or image-rays from a first-guess velocity model;
3. After generating a starting velocity-depth model, ray tracing is performed for calculating the kinematic FO CRS parameters along the central ray;
4. The paraxial FO CRS traveltime is used for calculating all the semblance values in all CMP gathers analyzed. If this coherence measure is maximum, the model is accepted and, the process is finished; otherwise, the process restarts from step 2 after updating the velocity, following the optimization strategy of the VFSA method. This algorithm is applied layer-by-layer (Mesquita et al., 2019).

According to Lima et al. (2011), we can give a statistical interpretation of the semblance function, which its general m-order form is given by

$$S_m(\mathbf{m}) = 1 - \frac{\sum_{k=-w}^{w}\left[\sum_{i=1}^{N}(a_{ik} - \mu_1)^m\right]}{\sum_{k=-w}^{w}\left[\sum_{i=1}^{N} a_{ik}^m\right]}, \quad (5)$$

where $a_{ik} = a_i(t_k)$, and μ_1 is the arithmetic mean of a set of amplitudes along the FO CRS traveltime curve.

We propose a slight modification in the semblance expression. This alternative objective function consists of changing the arithmetic mean measure in equation 5 by its median M. So, our m-order equation will be given by

$$\hat{S}_m(\mathbf{m}) = 1 - \frac{\sum_{k=-w}^{w}\left[\sum_{i=1}^{N}(a_{ik} - \mathrm{M})^m\right]}{\sum_{k=-w}^{w}\left[\sum_{i=1}^{N} a_{ik}^m\right]}. \quad (6)$$

This change in our tests showed that the farther the FO CRS traveltime curve is from the target event in the CMP gather, and therefore the more distant from the correct velocity of the model, the closer to zero the semblance value will be. For the case of higher-order semblances, the difference between the smallest and largest values increases.

Figure 1 shows a CMP gather acquired from a simple geologic model composed of a layer with constant velocity v_p = 1500 m/s and a plane-horizontal interface. The red curves represent the traveltimes for seven velocity-trials after applying the FO CRS tomography method. The calculation of μ_1 and M along these curves shows that $\mathrm{M} \ll \mu_1$ for distant values from the correct velocity.

To accurate our test, we carried out the inversion by applying it sequentially to velocities from 1200 m/s to 1800 m/s with a step of $dv = 2$ m/s. Figure 2 shows a comparison of μ_1 and M calculated along different traveltime curves for different velocities. It, consequently, affects the calculation of semblance function, causing the same effect, as we can see in applications.

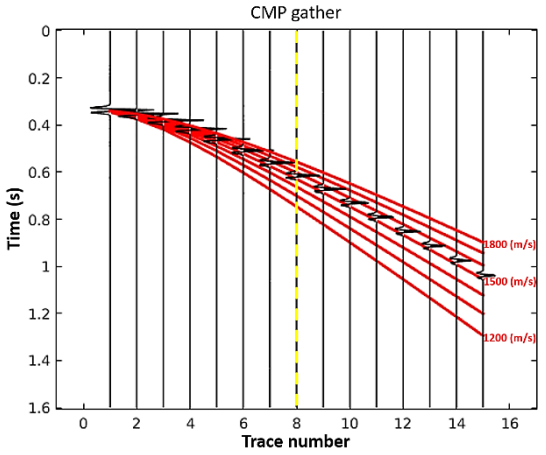

Figure 1. Traveltime curves for seven different velocities after applying FO CRS tomography method in a CMP gather. The yellow dashed line represents the FO traveltime of the central ray.

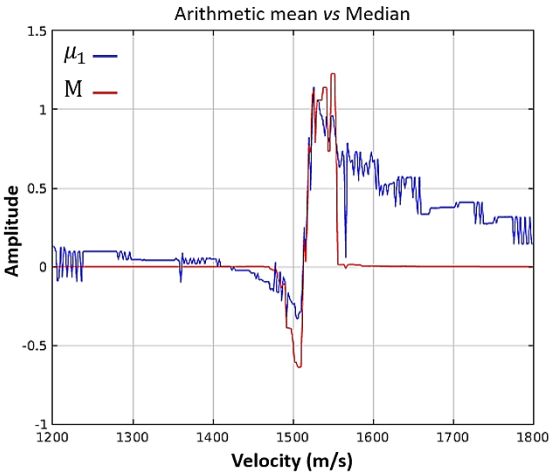

Figure 2. Comparison of μ_1 and M calculated along different traveltime curves for different velocities.

Applications

Synthetic case

We applied our proposed approach to a synthetic geological model composed of two homogeneous layers, which $v_1 = 1500$ m/s and $v_2 = 1800$ m/s, as shown in Figure 3. The yellow dashed line corresponds to the position of the CMP gather analyzed. In this example, we considered the stacked section for the FO CRS tomography application.

For the first layer, we choose a search range from 1200 m/s to 1800 m/s, with a step of 2 m/s increasingly. For the second layer, the search range was from 1700 m/s to 2100 m/s, with step of 5 m/s. We used S_2, $\hat{S}_2$, and $\hat{S}_4$ for the evaluations.

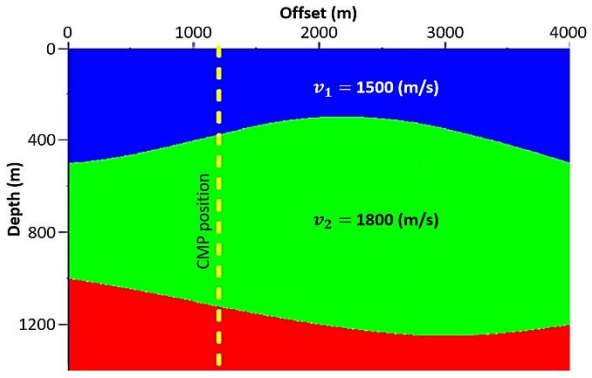

Figure 3. Synthetic geologic model. The yellow dashed line corresponds to the position of the CMP analyzed.

Field case

In the field example, we applied the FO CRS tomography to a seismic acquisition, line 50-RL-90, carried out in the Tacutu Basin, localized in northern Brazil. We choose the first layer from its time-migrated section interpretation (Figure 4), which corresponds to the area between the CMP gathers 1000 and 1420, and up to 0.5s. In all, 39 CMP gathers were analyzed.

Our objective in this application is to study the convergence of the inversion method by using E_2 and $\hat{E}_4$, which corresponds to equation 4 in a function of S_2, and $\hat{S}_4$, respectively.

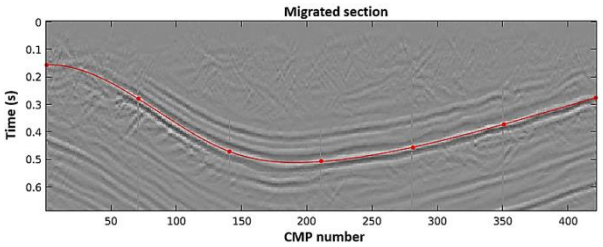

Figure 4. The selected region of the Tacutu seismic section. The red curve represents an interpreted interface.

Results and discussions

The results for the synthetic case are shown in the following six figures. Figure 5 shows our evaluation considering the conventional second-order semblance function S_2, according to described before. The estimated pair $(v_1, \max(S_2))$ is highlighted where semblance assumes the maximum value.

Figure 6 shows the result by considering $\hat{S}_2$ as the objective function. The effective region for analysis has been reduced to the range between 1440 m/s and 1520 m/s. Semblance values outside this range have been canceled or become negative. Then, Figure 7 presents our results by considering $\hat{S}_4$. In this case, the effective region was further reduced, between 1450 m/s and 1510 m/s, approximately.

From Figure 8 to Figure 10, we performed the same evaluations for layer 2. For both layers, we noticed the appearance of negative semblance values for studies with the median. For these cases, negative values can be considered null without affecting the velocity estimation process.

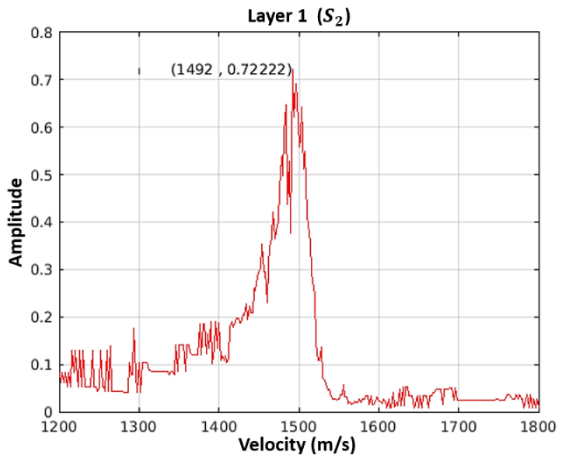

Figure 5. Evaluation of the conventional second-order semblance for layer 1 of the synthetic example. Highlighted, the estimated pair $(v_1, \max(S_2))$ where semblance assumes the maximum value.

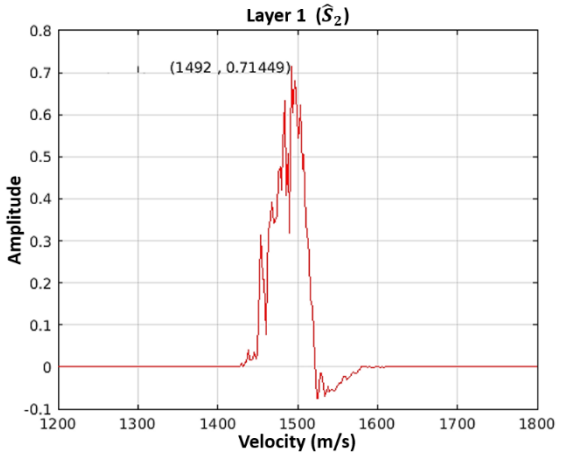

Figure 6. Result by considering $\hat{S}_2$ as the objective function for layer 1 of the synthetic example. Highlighted, the estimated pair $(v_1, \max(\hat{S}_2))$.

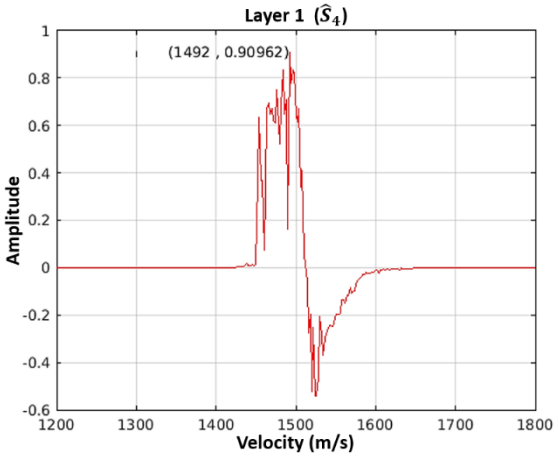

Figure 7. Result by considering $\hat{S}_4$ as the objective function for layer 1 of the synthetic example. Highlighted, the estimated pair $(v_1, \max(\hat{S}_4))$.

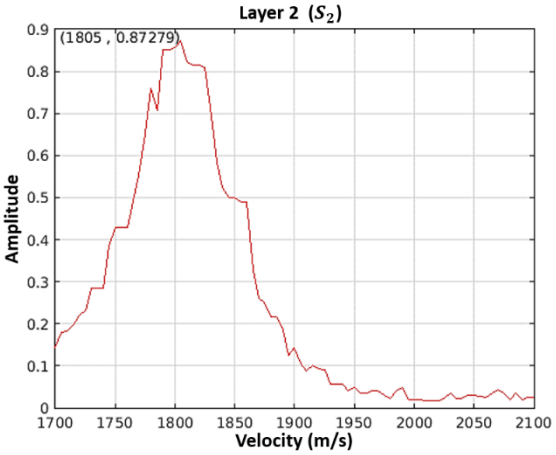

Figure 8. Evaluation of the conventional second-order semblance for layer 2 of the synthetic example. Highlighted, the estimated pair $(v_2, \max(S_2))$.

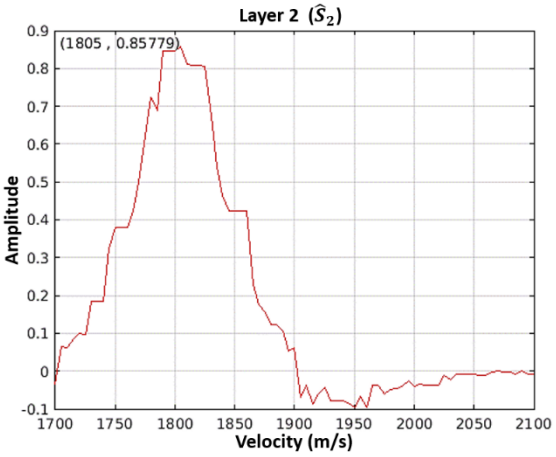

Figure 9. Result by considering $\hat{S}_2$ as the objective function for layer 2 of the synthetic example. Highlighted, the estimated pair $(v_2, \max(\hat{S}_2))$.

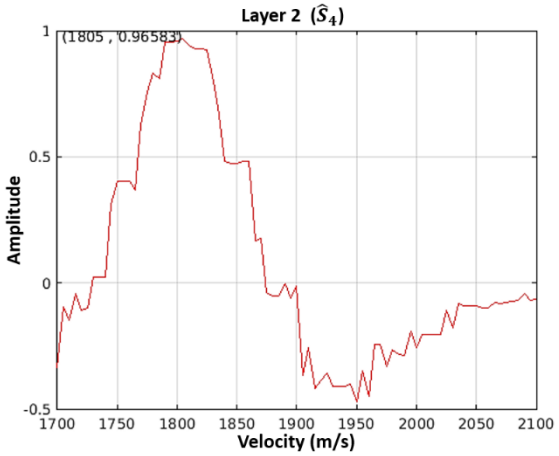

Figure 10. Result by considering $\hat{S}_4$ as the objective function for layer 2 of the synthetic example. Highlighted, the estimated pair $(v_2, \max(\hat{S}_4))$.

Figure 11 shows the results of the convergence study for the field case. E_2 is the objective function. In all, we carried out ten tests, in which the mean of the estimated velocities was 2167 m/s, with a standard deviation of 8.5764 m/s and the mean of maximum semblances of 0.5164. Figure 12 shows the result by considering $\hat{E}_4$ as the objective function. In this case, the means of the estimated velocities and the maximum semblances were 2187 m/s and 0.7086, respectively. The standard deviation was 6.4256 m/s. The last result shows that the search quickly displaces to closer where the maximum semblance is, restricting it mainly in this region.

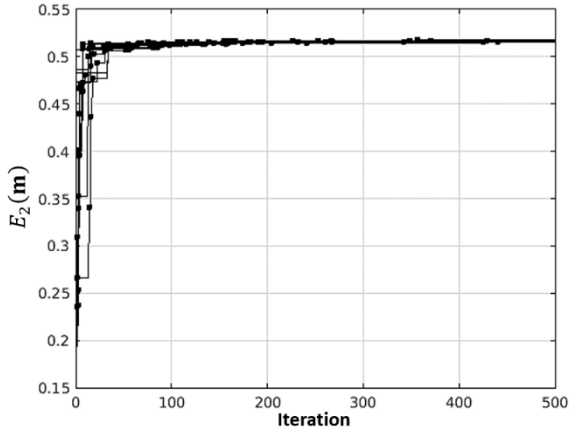

Figure 11. Result of the convergence analysis by applying the FO CRS tomography method and considering E_2 as the objective function. In all, we carried out ten tests.

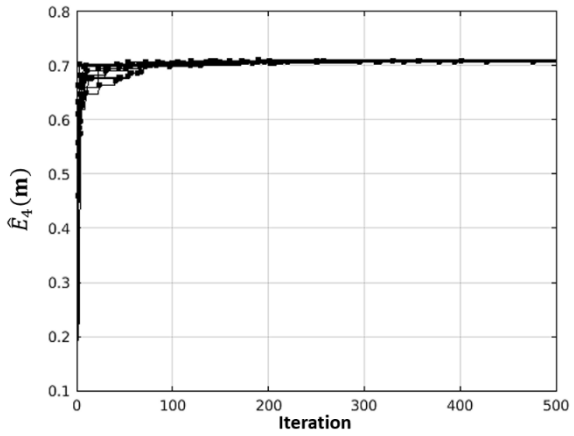

Figure 12. Result of the convergence analysis by considering $\hat{E}_4$ as the objective function. The search quickly displaces to closer where the maximum is.

Conclusions

We examine in this study an alternative form of the objective function of the FO CRS tomography method. Our analysis encourages using semblance with median since our results show that, in a certain way, the search concentrates in a limited region. It reduces the number of local maximum values, accelerating the convergence to the optimum value. Also, this approach can be advantageous in methods where local optimization using semblance is required.

Acknowledgments

The authors would like to thank CPGF/UFPA and CENPES/PETROBRAS for supporting in part these research activities.

References

BILLETTE, F., and LAMBARÈ, G., 1998, Velocity macro-model estimation by stereotomography: Geophysical Journal International, 135, 671–680, doi: 10.1046/j.1365-246X.1998.00632.x.

CALLAPINO, G. G.; OLIVA, P. C.; CRUZ, J. C. R., 2011, Numerical analysis of the finite-offset common-reflection-traveltime approximations. Journal of Applied Geophysics, n. 74, p. 89-99, doi: 10.1016/j.jappgeo.2011.03.005.

GOLDIN, S. V., 1979, Interpretation of seismic data: Nedra (English translation: seismic traveltime Inversion, 1986. SE8, Tulsa).

INGBER, L., 1989, Very fast simulated reannealing: Mathematical and Computer Modeling, 12, 967–993, doi: 10.1016/0895-7177(89)90202-1.

LIMA, E.; SANTOS, T. S.; SCHLEICHER, J.; TYGEL, M., 2011, A comparison of semblances of different order in common-reflection-surface parameter estimation. Journal of Geophysics and engineering, v. 8(2), p. 175-184, doi: 10.1088/1742-2132/8/2/005.

LU, W., LI, Y., ZHANG, S., XIAO, H., LI, Y., 2005, Higher-order-statistics and supertrace-based coherence-

estimation algorithm. Geophysics, v. 70(3), P13, doi: 10.1190/1.1925746.

MESQUITA, M. J. L., CRUZ, J. C. R., CALLAPINO, G. G., 2019, Velocity inversion by global optimization using-finite offset common-reflection-surface stacking applied to synthetic and Tacutu Basin seismic data. Geophysics, v. 84(2), R165-R174, doi: 10.1190/GEO2017-0117.1.

NEIDELL, N. S., and TANER, M. T., 1971, Semblance and other coherency measures for multichannel data: Geophysics, 36, 482–497, doi: 10.1190/1.1440186.

TARANTOLA, A., 1984, Inversion of seismic reflection data in the acoustic approximation: Geophysics, 49, 1259–1266, doi: 10.1190/1.1441754.

WIGGINS, R., 1978, Minimum entropy deconvolution: Geoexploration, 16, 21-35, doi: 10.1016/0016-7142(78)90005-4.

ZHANG, Y.; BERGLER, S.; HUBRAL, P., 2001, Common-Reflection-Surface (CRS) stack for common-offset. Geophy. Prospect., 49, 709-718, doi:10.1046/j.1365-2478.2001.00292.x.